Cement and Concrete Composites 139 (2023) 104996

Contents lists available at ScienceDirect

Cement and Concrete Composites

journal homepage: www.elsevier.com/locate/cemconcomp

Cracking failure behavior of high strength concrete containing nano-$CaCO_3$ at early age

Dejian Shen [a,b,c,*], Jiacheng Kang [a,b,c], Haoze Shao [a,b,c], Ci Liu [a,b,c], Ming Li [a,b,c], Xusheng Chen [a,b,c]

[a] College of Civil and Transportation Engineering, Hohai Univ, No. 1, Xikang Rd., Nanjing, 210024, China
[b] Jiangsu Engineering Research Center for Crack Control in Concrete, No. 1, Xikang Rd., Nanjing, 210024, China
[c] Nanjing Engineering Research Center for Prefabricated Construction, No. 1, Xikang Rd., Nanjing, 210024, China

ARTICLE INFO

Author keywords:
High strength concrete
Nano-$CaCO_3$
Tensile creep
Restrained cracking
Temperature stress test machine
Early age

ABSTRACT

Nano-calcium carbonate ($CaCO_3$) has been added to high strength concrete (HSC) to reduce cement usage, control greenhouse gas emissions, increase durability, and control excessive shrinkage of HSC. Many investigations on the mechanical properties and shrinkage of HSC containing nano-$CaCO_3$ have conducted. However, the early-age cracking failure behavior of that considering temperature, shrinkage, restrained stress, and tensile creep simultaneously was rarely investigated. Temperature stress test machine, which could measure these factors simultaneously, was used to investigate the influence of nano-$CaCO_3$ contents (0%, 1%, 2%, and 3% by weight of cement powder) on the early-age cracking failure behavior of HSC in the present investigation. Mechanical properties of HSC containing nano-$CaCO_3$ were tested. The addition of nano-$CaCO_3$ to HSC improved the mechanical properties, and reduced the tensile creep as well as autogenous shrinkage of that at early age. A simplified stress-strain failure criterion was proposed.

1. Introduction

High strength concrete (HSC) with diverse sources, good durability, and relatively low cost has been applied in construction practices widely. However, environmental pollution as well as resource consumption is inevitable with the wide application of concrete. As an important raw material for producing HSC, the production of cement consumes great energy resource, and simultaneously would generate much carbon dioxide (CO_2) [1]. At the same time, the typically low water-binder (w/b) ratio would cause self-desiccation in HSC [2–4]. Autogenous shrinkage would be caused by self-desiccation, and restrained cracking commonly occurs in the HSC structures under restraint conditions. When cracking occurs, the aggressive substances can easily penetrate concrete, which would affect the quality of concrete and cause many security problems [5]. Thus, investigations on the cracking problem of HSC are necessary for ensuring the safety of concrete structures.

In recent years, nano-sized materials have attracted much attention due to their excellent properties, and many nano-sized materials have been incorporated into cement-based composites to modify their properties. Many studies have revealed that nano-sized materials have a better effect on concrete than micro counterparts [6,7]. Nano-calcium carbonate ($CaCO_3$) is a kind of nano-sized materials, and the incorporation of nano-$CaCO_3$ has been an effective method to reduce the use of cement and control greenhouse gas emissions [8]. Moreover, the incorporation of nano-$CaCO_3$ would increase durability, and control excessive shrinkage of concrete when the mix design is proper [9]. Recent years have seen increased attention being given to the cementitious composites containing nano-$CaCO_3$. Liu et al. [10] investigate the flexural strength, compressive strength, and autogenous shrinkage strain of cement paste containing nano-$CaCO_3$, and reveal that the optimum content of nano-$CaCO_3$ in cement paste is 1%. Cao et al. [7] point out that the chemical and physical effects of nano-$CaCO_3$ on concrete are more effective than that of micro-$CaCO_3$, and the enhancement effect of nano-$CaCO_3$ is reduced due to agglomeration. Meng et al. [11] reveal that nano-$CaCO_3$ is helpful to increase the mechanical properties due to the seeding effect and filler effect. Sato and Diallo [12] find out that hydration of tricalcium silicate in concrete is accelerated due to the seeding effect of nano-$CaCO_3$. Liu et al. [13] report that adding nano-$CaCO_3$ decrease autogenous shrinkage of cement-based materials by

* Corresponding author. College of Civil and Transportation Engineering, Hohai Univ, No. 1, Xikang Rd., Nanjing, 210024, China.
E-mail address: shendjn@163.com (D. Shen).

https://doi.org/10.1016/j.cemconcomp.2023.104996
Received 16 June 2021; Received in revised form 7 January 2023; Accepted 19 February 2023
Available online 22 February 2023

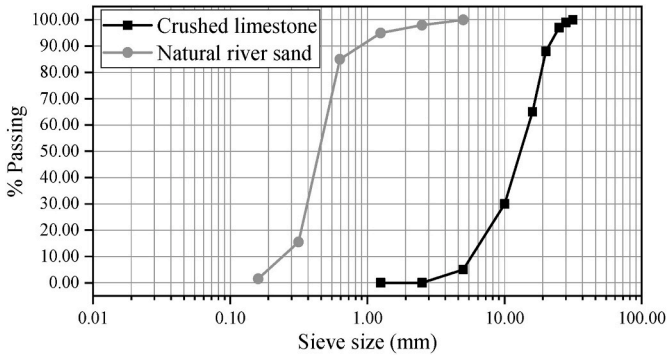

Fig. 1. Particle size distribution curves of aggregates.

Table 1
Chemical compositions and properties of Portland cement.

Item	Portland cement
SiO_2 (%)	19.90
Al_2O_3 (%)	4.60
Fe_2O_3 (%)	3.00
CaO (%)	64.60
MgO (%)	0.78
SO_3 (%)	2.37
Na_2O (%)	0.06
K_2O (%)	0.65
Specific surface area (m^2/g)	375

Table 2
Chemical compositions and properties of nano-$CaCO_3$.

Item	nano-$CaCO_3$
$CaCO_3$ (%)	≥98
MgO (%)	≥0.5
SiO_2 (%)	≥0.1
Al_2O_3 (%)	≥0.1
Fe_2O_3 (%)	≥0.1
Specific surface area (m^2/g)	40

Table 3
Mix proportions and properties of concrete.

Component	NC-00	NC-01	NC-02	NC-03
Water (kg/m^3)	151.8	151.8	151.8	151.8
Cement (kg/m^3)	460.0	455.4	450.8	446.2
Nano-$CaCO_3$ (kg/m^3)	0	4.6	9.2	13.8
Fine aggregate (kg/m^3)	670.6	670.6	670.6	670.6
Coarse aggregate (kg/m^3)	1117.6	1117.6	1117.6	1117.6
Superplasticizer (kg/m^3)	2.07	2.07	2.07	2.07
Initial setting time (h)	6.68	6.42	6.18	5.94
Final setting time (h)	10.35	9.95	9.58	9.21
Workability (mm)	153	137	130	120
Specific weight (kg/m^3)	2478	2465	2453	2438
Air content at fresh state (%)	1.65	1.89	1.49	1.39

decreasing the porosity and reacting with tricalcium aluminate. The early-age restrained cracking is generally affected by shrinkage-induced stress in tension. The tensile creep is an important factor in evaluating restrained stress accurately [14–16]. Thus, the determination of tensile creep is significant in evaluating early-age restrained cracking failure behavior of concrete. However, the determination of tensile creep is complicated for early-age concrete because the physical and chemical properties change simultaneously at early age [14]. Little literature has been published on early-age tensile creep of HSC containing nano-$CaCO_3$. Thus, investigations on tensile creep are necessary for better understanding the cracking failure behavior of HSC containing nano-$CaCO_3$ at early age.

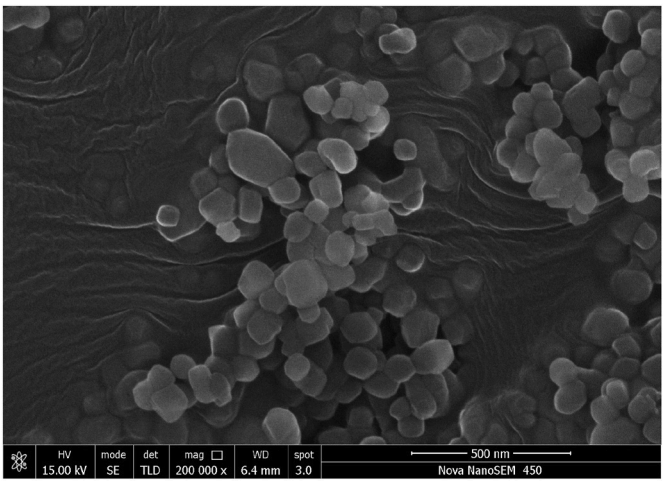

Fig. 2. SEM morphology of nano-$CaCO_3$ powders.

As an effective method to estimate cracking resistance of concrete, temperature stress test machine (TSTM) could study various behavior of concrete under uniaxial restraint conditions, e.g., temperature, shrinkage, restrained stress, and creep [17,18]. In addition, the simulation of internal condition of mass concrete can be conducted by TSTM by providing a nearly adiabatic condition [19]. Kovler [20] determines the tensile creep of concrete based on results obtained by free and restrained specimens of TSTM. Klausen et al. [21] study the cracking behavior of concrete containing fly ash using TSTM test, and reveal that the cracking occurs when restrained stress of concrete reaches around 80% of its tensile strength. Several criteria, e.g., cracking stress [22], cracking age [23], ratio of cracking stress to tensile strength [24], stress reserve [25,26], as well as the integrated criterion [27,28], have been suggested by researchers to estimate cracking failure behavior of concrete. Cracking resistance of different concrete mixtures could be compared by these criteria. However, cracking resistance of single concrete mixture fails to be evaluated by these criteria. Thus, proposing a criterion for evaluating the cracking failure behavior of single concrete mixture is necessary.

In the present investigation, the influence of nano-$CaCO_3$ on tensile creep and cracking failure behavior of HSC at early age was investigated. The mechanical properties, temperature history, autogenous shrinkage, restrained stress, and tensile creep of HSC containing different nano-$CaCO_3$ contents (0%, 1%, 2%, and 3% by weight of cement powder) were tested. The prediction models of mechanical properties and the simplified stress-strain failure criterion of HSC containing nano-$CaCO_3$ were proposed.

2. Details of experiments

2.1. Materials

In the present investigation, ingredient materials of HSC matrix were P•II 52.5 R Portland cement (China Standard GB 175 [29] and ASTM C150 [30]), river sand (fineness modulus was 2.05), and crushed limestone (maximum aggregate size was 28 mm), polycarboxylate-based superplasticizer, and tap water. Nano-$CaCO_3$ powder (average size was 40 nm, and $CaCO_3$ content was 98%) was used to replace part of the cement in HSC matrix. The particle size distribution curves of aggregates was given in Fig. 1. Table 1 and Table 2 depict chemical compositions and properties of Portland cement and the nano-$CaCO_3$, respectively.

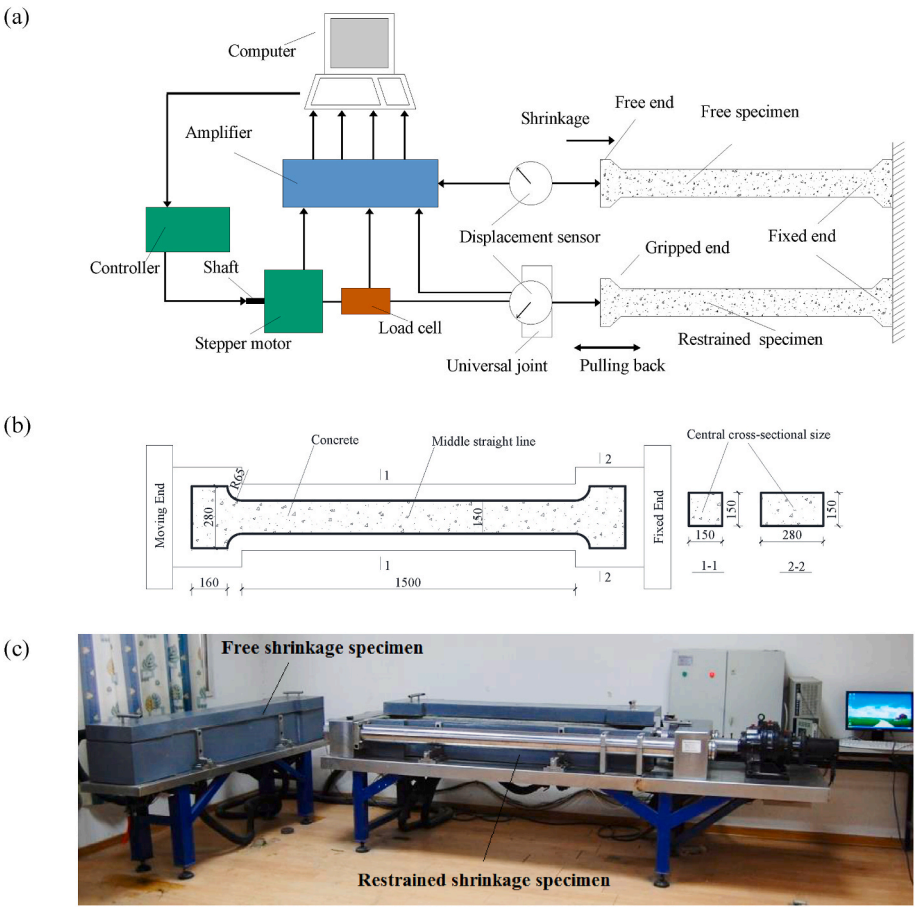

Fig. 3. The schematic diagrams of TSTM: (a) The schematic diagram of TSTM [20]; (b) The schematic diagram of specimen mold (mm); (c) The photo of TSTM.

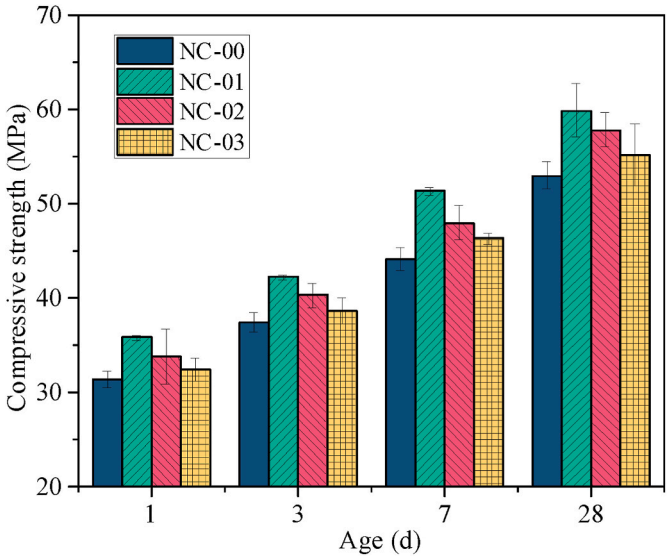

Fig. 4. Results of compressive strength obtained from experiment.

2.2. Mixture proportions

In the present investigation, nano-$CaCO_3$ of 1%, 2%, and 3% by weight of cement powder were prepared as Mixture NC-01, NC-02, and NC-03, respectively, and a reference concrete without nano-$CaCO_3$ was prepared as NC-00. The w/b ratio was 0.33 for four mixtures, and Table 3 depicts the mix proportions and properties of four mixtures. The binder content composed of the cement and nano-$CaCO_3$, and the total mass of the cement and nano-$CaCO_3$ were kept constant to maintain the same w/b ratio in four mixtures. The nano-$CaCO_3$ was in the form of white powder, and the nano-$CaCO_3$ powders imaged with the Scanning Electron Microscope (SEM) were in cubic crystalline shape, as depicted in Fig. 2.

2.3. Experimental procedure

2.3.1. Mechanical properties test

Specimens for mechanical properties test were molded and cured on the 20 °C condition. The tests of compressive strength, splitting tensile strength, and elastic modulus at the age of 1, 3, 7, and 28 d after casting were conducted according to China Standard GB/T 50081 [31]. Three samples were prepared for each test at a certain age, and results of mechanical properties were determined by the average value of three samples. The sample size was 150 mm × 150 mm × 150 mm for compressive and splitting tensile strength test, and was 150 mm × 150 mm × 300 mm for elastic modulus test.

2.3.2. TSTM test

The concrete from early-age in free and restraint conditions can be characterized by TSTM system [32]. As depicted in Fig. 3(a), TSTM is equipped with measuring and controlling systems of temperature, displacement, and load [33]. TSTM specimen molds were both in dog-bone shape, and the dimension at the central part was 150 mm × 150 mm × 1500 mm, as depicted in Fig. 3(b). Fig. 3(c) depicts the photo of TSTM.

The process of TSTM test was as follows: 1) Concrete mixtures were cast into the TSTM specimen molds, and the surface of concrete was

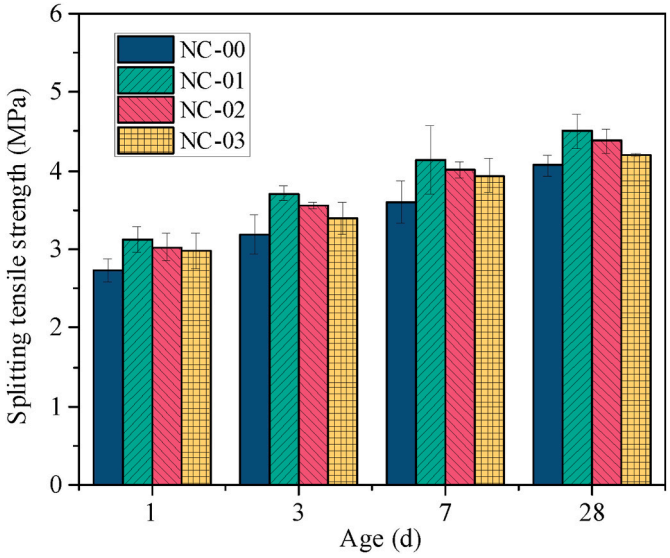

Fig. 5. Results of splitting tensile strength obtained from experiment.

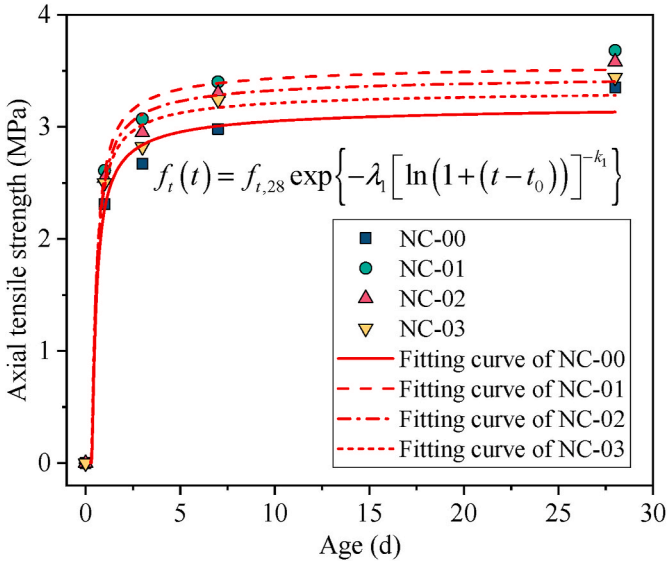

Fig. 6. Results of prediction model of axial tensile strength.

sealed to prevent moisture from evaporating. 2) Temperature sensors were installed at the center of restrained shrinkage and free shrinkage specimen molds to record temperature history of concrete. Molds were hollow and filled with ethylene glycol to control temperature of concrete. Adiabatic curing mode was conducted to simulate the condition of mass concrete, as reported in Refs. [19,34–38]: the concrete increased to peak temperature, and was maintained for 48 h. Finally, the concrete cooled down at a rate of 1 °C/h until cracking. 3) Displacement sensors with accuracy of 0.01 μm were installed to determine the displacement of two specimen molds. 4) Once displacement of restrained specimen reached a threshold value (2 μm), the specimen was pulled/pushed to original position by a stepper motor to provide full restraint, as reported in Refs. [39,40]. The displacement of the free specimen mold was not under restraint condition. 5) The measurements started immediately after pouring, and the data was collected until concrete cracked. The test data was obtained every 5 min. One TSTM test was conducted for each mixture in the present investigation, as recommended in Refs. [20,41].

3. Test results and discussion

3.1. Mechanical properties

3.1.1. Compressive strength

The compressive strength of four concrete mixtures is depicted in Fig. 4. It is remarked that partial replacement of cement by nano-$CaCO_3$ improved compressive strength of HSC. For example, the 28-d compressive strength was 53.0, 59.9, 57.8, and 55.2 MPa, which increased by 13.0%, 9.1%, and 4.2% with increasing content of nano-$CaCO_3$ ranging from 0% to 1%, 2%, and 3%, respectively. Result also reveals that the increase ratio of HSC containing 1% nano-$CaCO_3$ in compressive strength was higher than that of HSC containing 2% and 3% nano-$CaCO_3$ at different ages. Similar findings on the compressive strength can be found in the literature [10,42]. Liu et al. [10] reveal that the addition of nano-$CaCO_3$ enhanced the 7-d and 28-d compressive strength of hardened cement paste. Shaikh et al. [42] study the compressive strength of concrete containing different nano-$CaCO_3$ contents ranging from 1% to 4%, and results reveal that the concrete containing 1% nano-$CaCO_3$ showed the highest compressive strength.

3.1.2. Tensile strength

The partial replacement of cement in concrete by nano-$CaCO_3$ enhanced its splitting tensile strength, as depicted in Fig. 5. For example, the 28-d splitting tensile strength was 4.07, 4.50, 4.38, and 4.20 MPa, which increased by 10.6%, 7.6%, and 3.2% with increasing content of nano-$CaCO_3$ ranging from 0% to 1%, 2%, and 3%, respectively.

Splitting tensile strength of HSC containing 1% nano-$CaCO_3$ reached maximum, and decreased when the content of nano-$CaCO_3$ was beyond 1%. Similar findings on tensile strength can be found in the literature [43]. Mishra et al. [43] find that the tensile strength increases with the increment of nano-$CaCO_3$ due to the formation of small spherulites in concrete.

Time-dependent axial tensile strength was calculated using Eqs. (1) and (2) in the present investigation, as reported in Refs. [44,45].

$$f_t = 0.77 \times f_{spl} + 0.21 \tag{1}$$

$$f_t(t) = f_{t,28}\exp\left\{-\lambda_1[\ln(1+(t-t_0))]^{-k_1}\right\} \tag{2}$$

where f_t = axial tensile strength, in MPa; f_{spl} = splitting tensile strength, in MPa; $f_t(t)$ = time-dependent axial tensile strength, in MPa; $f_{t,28}$ = 28-d axial tensile strength, in MPa; t = age of concrete after casting, in day; t_0 = initial setting time of concrete, in day; and λ_1, k_1 = fitting parameters. Results of prediction model of axial tensile strength are depicted in Fig. 6 and Table 4, and the coefficients of determination (R^2) were over 0.980. The setting times of concrete were also tested in the present investigation. The results of initial setting time or final setting time were 6.68, 6.42, 6.18, and 5.94 h or 10.35, 9.95, 9.58, and 9.21 h, which decreased by 3.9%, 7.5%, and 11.1% or 3.9%, 7.4%, and 11.0% with increasing content of nano-$CaCO_3$ ranging from 0% to 1%, 2%, and 3%, respectively, as depicted in Table 3. The addition of nano-$CaCO_3$ can shorten the setting time of concrete because they have a larger surface area than larger particles. The larger the surface area of nano-$CaCO_3$, the more water they can come into contact with, and the faster the hydration reaction will occur.

3.1.3. Elastic modulus

Fig. 7 depicts that partial replacement of cement in concrete by nano-$CaCO_3$ enhanced its elastic modulus. For example, the 28-d elastic modulus was 50.2, 56.2, 55.6, and 52.7 GPa, which increased by 12.0%, 10.8%, and 5.0% with increasing content of nano-$CaCO_3$ ranging from 0% to 1%, 2%, and 3%, respectively. Similar findings on elastic modulus can be found in the literature [46]. A possible explanation for this might be that the nucleation of calcium silicate hydrate (C-S-H) is accelerated due to the seeding effect of nano-$CaCO_3$ [46]. Considering that the

Table 4
Results of axial tensile strength and elastic modulus.

Concrete mixtures	Axial tensile strength (MPa)				λ_1	k_1	Elastic modulus (GPa)				λ_2	k_2
	1 d	3 d	7 d	28 d			1 d	3 d	7 d	28 d		
NC-00	2.31	2.67	2.98	3.34	0.213	0.989	33.2	46.4	48.7	50.2	0.126	1.954
NC-01	2.61	3.07	3.40	3.68	0.183	1.115	35.8	52.0	54.2	56.2	0.134	2.026
NC-02	2.54	2.95	3.30	3.58	0.189	1.088	35.7	51.6	53.6	55.6	0.132	2.053
NC-03	2.50	2.82	3.24	3.44	0.178	1.098	35.2	48.5	51.9	52.7	0.124	2.044

*The results listed were the average value of three samples.

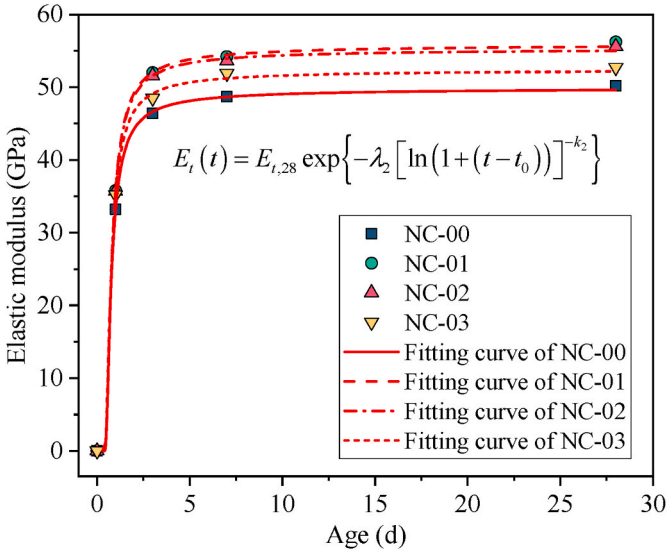

Fig. 7. Results of prediction model of elastic modulus.

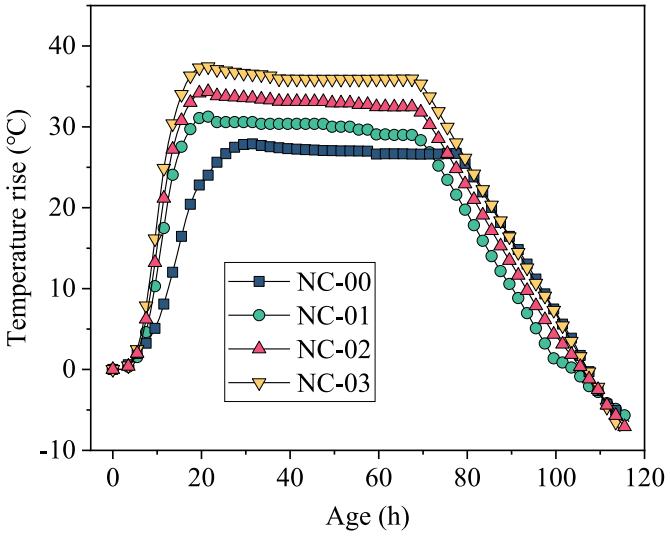

Fig. 8. Adiabatic temperature history of restrained specimen.

results of tensile elastic modulus are similar to compressive one at early age [47–49], Eq. (3) is used to predict time-dependent tensile elastic modulus on the basis of the results of compressive elastic modulus [45].

$$E_t(t) = E_{t,28}\exp\left\{-\lambda_2[\ln(1+(t-t_0))]^{-k_2}\right\} \quad (3)$$

where $E_t(t)$ = time-dependent tensile elastic modulus, in GPa; $E_{t,28}$ = 28-d tensile elastic modulus, in GPa; and λ_2, k_2 = fitting parameters. Table 4 depicts the results of prediction model of elastic modulus, and the results of R^2 were over 0.990.

The improvement of strength and modulus is attributed to two reasons: on one hand, the partial replacement of cement by nano-$CaCO_3$ accelerates the cement hydration and increases reaction products that enhance the microstructures [22]. On the other hand, the microstructure of concrete is filled up by adding nano-$CaCO_3$, which decreases the porosity and increases the density degree of concrete [23].

The replacement of cement with 1% nano-$CaCO_3$ showed a higher compressive strength, tensile strength, and elastic modulus than that of concrete containing 2% and 3% nano-$CaCO_3$. The reduced strength and elastic modulus are attributed to several factors. Firstly, the content of hydration products decreased due to the dilution effect caused by excessive nano-$CaCO_3$. Secondly, the space in concrete was filled up by adding nano-$CaCO_3$, and the formation of hydration products was impeded. Lastly, van der Waal's forces of nano-$CaCO_3$ are higher than that of cement powder in the wet mix, hence, weak zones are established in the microstructure of concrete because of the agglomeration of nano-$CaCO_3$ [42,50].

3.2. *Influence of nano-$CaCO_3$ on temperature history*

The heat induced by cement hydration in concrete would contribute to a quick temperature rise in concrete, which directly affects its cracking failure behavior at early age [51–53]. In the present investigation, casting temperature or peak temperature was 21.9, 20.7, 21.4, and 22.0 °C or 49.8, 52.0, 55.7, and 59.5 °C for Mixture NC-00, NC-01, NC-02, and NC-03, respectively. Adiabatic temperature rise is determined by Eq. (4) [54].

$$T_{tr} = T_{ht} - T_{ct} \quad (4)$$

where T_{tr} = adiabatic temperature rise, in °C; T_{ht} = peak temperature, in °C; and T_{ct} = casting temperature, in °C.

Fig. 8 depicts that adiabatic temperature rise was 27.9, 31.3, 34.3, and 37.5 °C for Mixture NC-00, NC-01, NC-02, and NC-03, which increased by 12.2%, 22.9%, and 34.4% with increasing content of nano-$CaCO_3$ ranging from 0% to 1%, 2%, and 3%, respectively. Besides, temperature rise rate increased by adding nano-$CaCO_3$, as depicted in Fig. 8, which was due to the filling and chemical effects of nano-$CaCO_3$. Similar findings can be found in the literature [46,55]. Sato et al. [46] and Camiletti et al. [55] both find that the hydration of cement is significantly accelerated by adding nano-$CaCO_3$. When the nano-$CaCO_3$ is in contact with water in the concrete mixture, on one hand, the Ca^{2+} around C_3S particles is absorbed onto the surface of nano-$CaCO_3$. On the other hand, the carboaluminates ($C_3A{\cdot}CaCO_3{\cdot}11H_2O$) are formed when CO_3^{2-} reacts with C_3A, which makes it easy for Ca^{2+} as well as water to diffuse into concrete. The two factors would reduce Ca^{2+} concentration, and increase hydration rate [56].

Early-age cracking resistance is directly affected by the tensile stress induced by temperature drop during cooling phase [57]. Temperature drop is taken to evaluate the cracking behavior of concrete in the present investigation, as reported in Ref. [58]. Eq. (5) is used to calculate temperature drop of HSC [59].

$$T_{td} = T_{ht} - T_{ck} \quad (5)$$

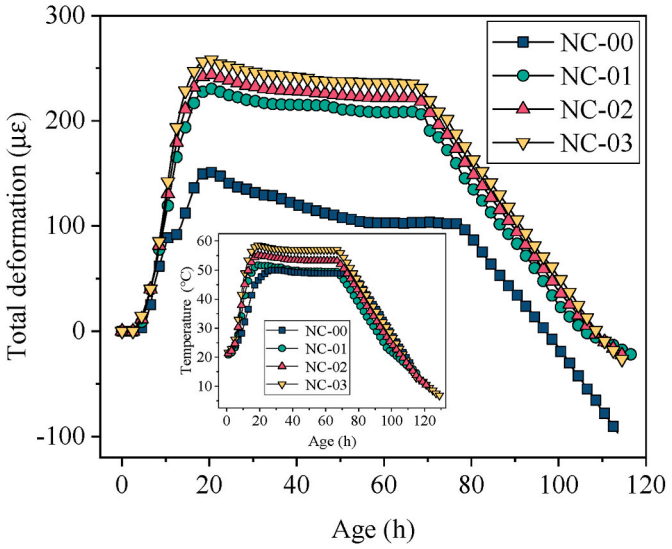

Fig. 9. Total deformation and temperature history recorded in free specimens.

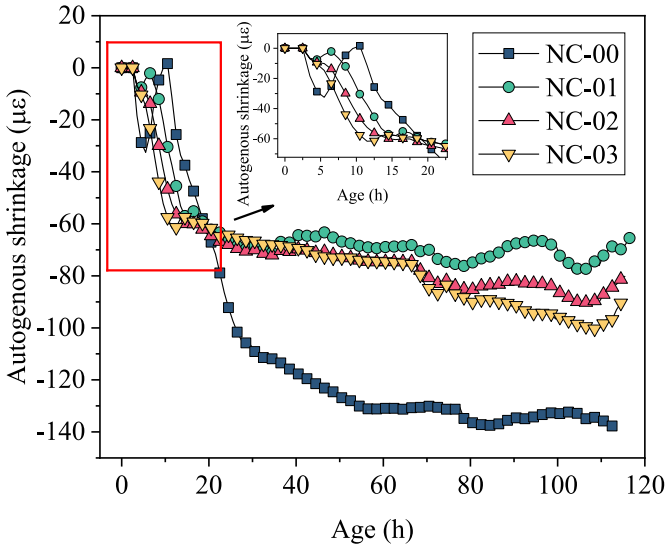

Fig. 10. Autogenous shrinkage of HSC containing nano-$CaCO_3$.

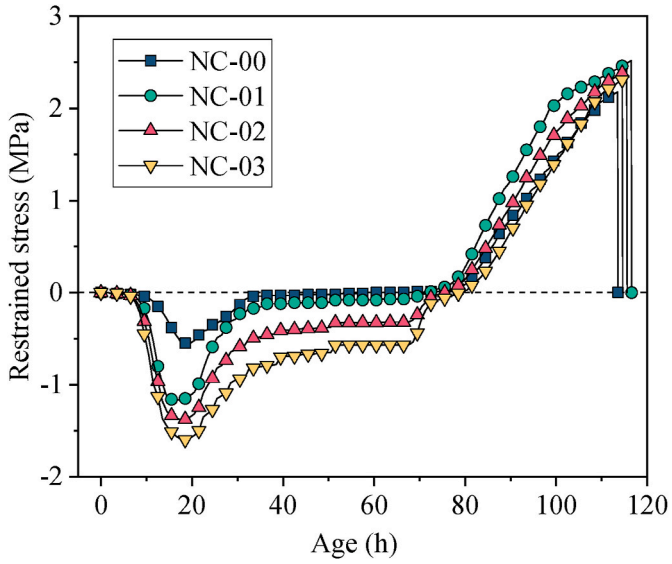

Fig. 11. Restrained stress recorded in restrained specimens.

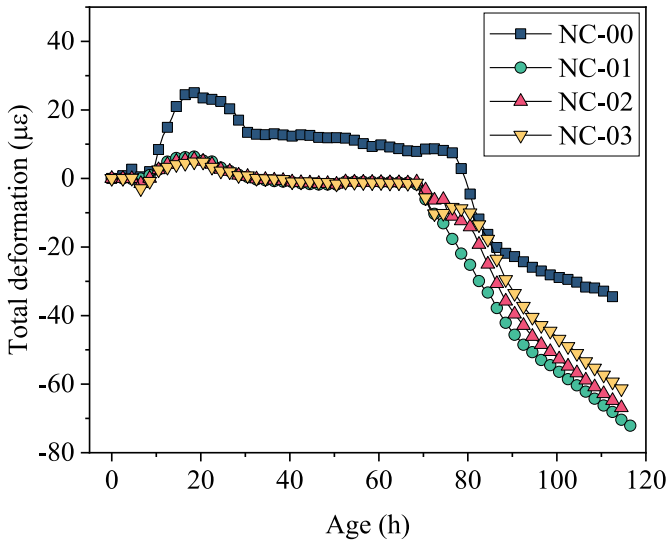

Fig. 12. Total accumulated deformation recorded in restrained specimens.

where T_{td} = temperature drop, in °C; T_{ht} = peak temperature, in °C; and T_{ck} = cracking temperature, in °C.

Results of cracking temperature or temperature drop were 16.9, 14.2, 14.3, and 14.3 °C or 32.9, 37.8, 41.4, and 45.2 °C for Mixture NC-00, NC-01, NC-02, and NC-03, which decreased by 16.0%, 15.4%, and 15.4% or increased by 14.9%, 25.8%, and 37.4% with increasing content of nano-$CaCO_3$ ranging from 0% to 1%, 2%, and 3%. Temperature drop improved when the cement in concrete was partly replaced by nano-$CaCO_3$, which indicated that the addition of nano-$CaCO_3$ to HSC reduced its thermal cracking risk.

3.3. *Influence of nano-$CaCO_3$ on autogenous shrinkage*

In the present investigation, the total deformation and temperature history of free specimen were measured, which includes autogenous shrinkage and thermal deformation [41]. Fig. 9 depicts the total deformation and temperature history recorded in free specimens. The analysis of deformation is implemented from "time-zero", and previous studies take different methods to determine "time-zero" [60–65]. Lura et al. [65] use TSTM to investigate the early-age shrinkage of concrete from the time when stress first occurs. Considering that only the stress-induced deformation was analyzed in the present investigation, the value of autogenous shrinkage was set to be zero from the beginning of the test to the point of "time-zero", as recommended in Ref. [65]. The deformation of free specimens increased at early stage after casting because of the temperature rise of concrete. Fig. 9 depicts that deformation of free specimens decreased gradually during constant temperature phase, and main reason was that thermal deformation remained constant, and autogenous shrinkage developed gradually in free specimens during this phase. When the concrete cooled down, the total deformation decreased continuously, and finally changed from expansion to contraction.

Autogenous shrinkage is considered as shrinkage that excludes volume changes induced by temperature variation, restraint, and loading [66,67]. Eq. (6) is used to subtract thermal deformation in order to determine autogenous shrinkage [68].

$$\begin{cases} \varepsilon_{as} = \varepsilon_{total} - \varepsilon_T \\ \varepsilon_T = \alpha \times \Delta T \end{cases} \tag{6}$$

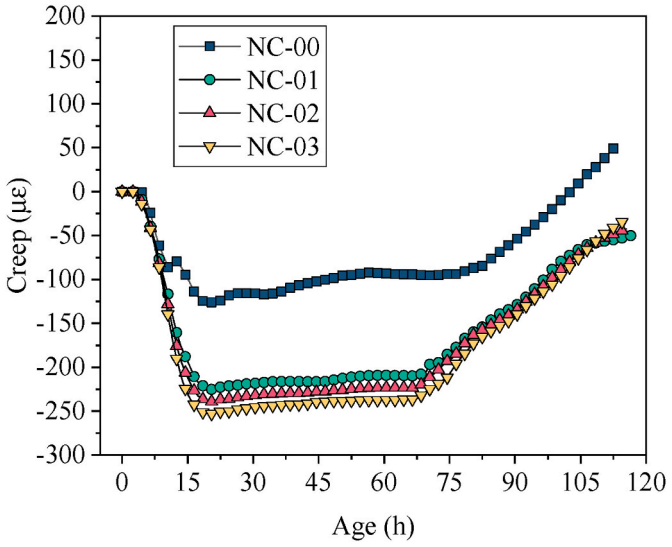

Fig. 13. Development of creep of HSC containing nano-$CaCO_3$.

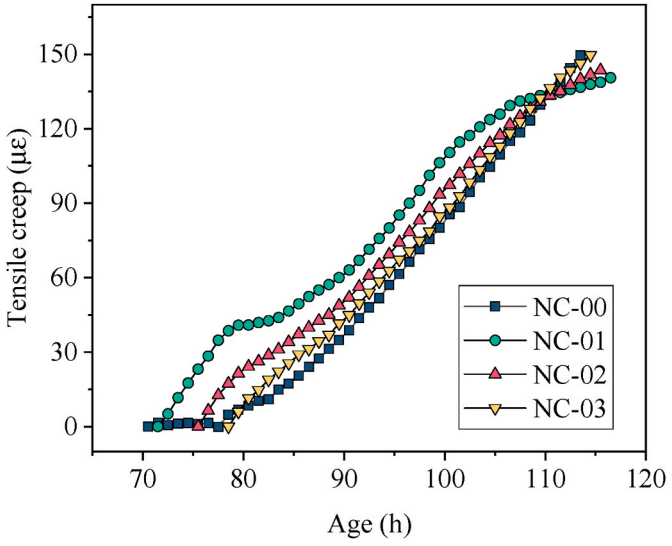

Fig. 14. Development of tensile creep of HSC containing nano-$CaCO_3$.

where ε_{total} = total deformation, in με; ε_{as} = autogenous shrinkage, in με; ε_T = thermal deformation, in με; α = coefficient of thermal expansion (CTE); and ΔT = temperature change, in °C.

CTE changes drastically along with time, and Eq. (7) is taken to calculate CTE to calculate the autogenous shrinkage more accurately [39].

$$\alpha_T(t) = \alpha_k \times (1 + 41 \times t^{-m}) \tag{7}$$

where $\alpha_T(t)$ = time-dependent CTE, in με/°C; α_k = 28-d CTE, in με/°C; and m = 2.0. The value of α_k was 6.04, 6.65, 6.23, and 5.80 με/°C for Mixture NC-00, NC-01, NC-02, and NC-03, respectively, which was calculated by regression analysis on results of free deformation and temperature history during cooling phase, as reported in Ref. [57]. Eq. (8) is used to determine autogenous shrinkage [68].

$$\varepsilon_{as}(t) = \varepsilon_{total} - \alpha_T(t) \times [T(t) - T_{time-zero}] \tag{8}$$

where $\varepsilon_{as}(t)$ = time-dependent autogenous shrinkage, in με; $T(t)$ = time-dependent temperature, in °C; and $T_{time-zero}$ = "time-zero" temperature, in °C.

Fig. 10 depicts the development of autogenous shrinkage of Mixture

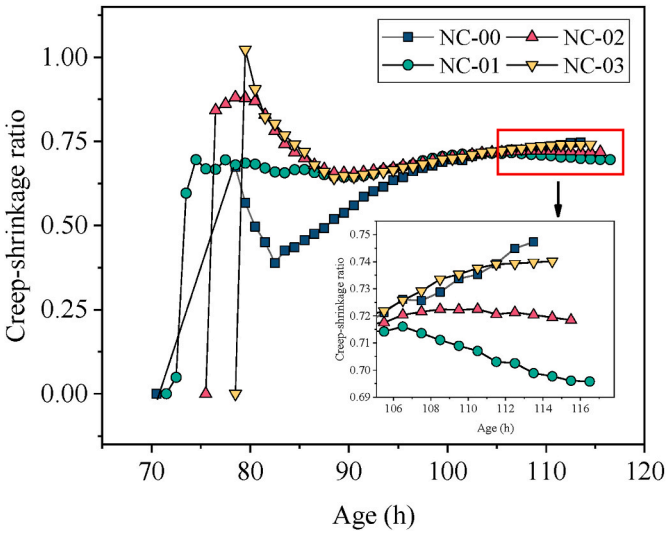

Fig. 15. Development of creep-shrinkage ratio of HSC containing nano-$CaCO_3$.

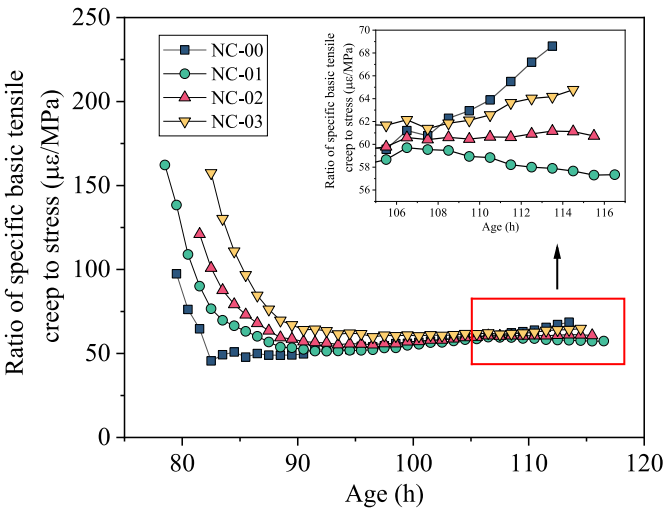

Fig. 16. Development of ratio of specific basic tensile creep to stress of HSC containing nano-$CaCO_3$.

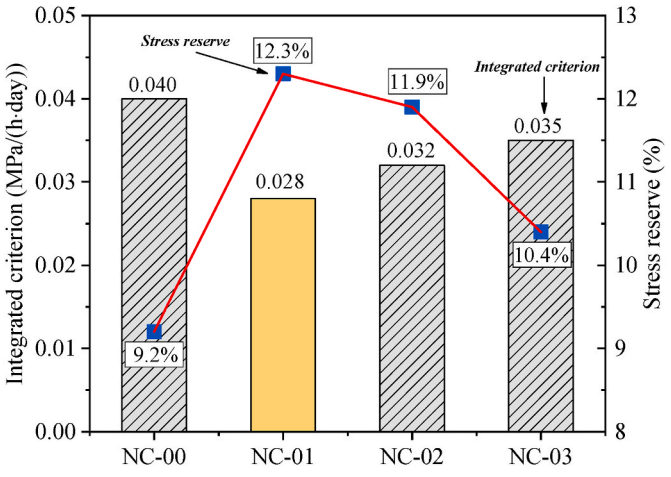

Fig. 17. Stress reserve and integrated criterion of HSC containing nano-$CaCO_3$.

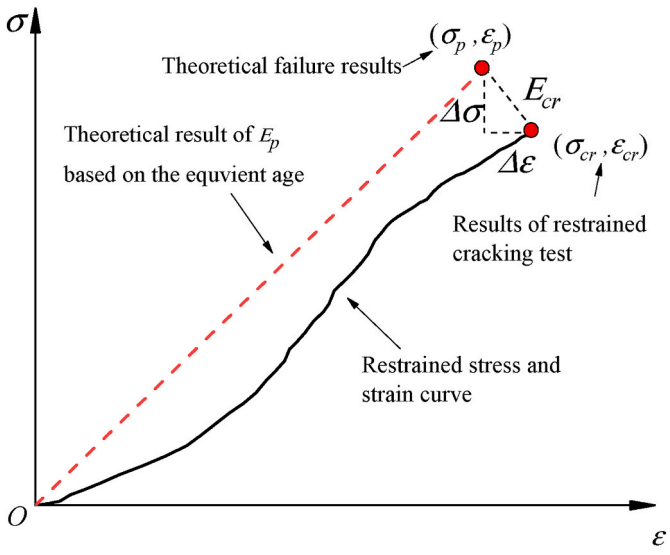

Fig. 18. Stress-strain relationship between theoretical failure results and results of restrained cracking test.

Table 5
Experimental and predicted results.

Concrete mixtures	Restrained specimen		Theoretical results		$K = \frac{\sigma_{cr}}{\sigma_p}$	σ_{pre}	$\frac{\sigma_{pre} - \sigma_{cr}}{\sigma_{cr}}$
	σ_{cr}	ε_{cr}	σ_p	ε_p			
NC-00	2.18	50.57	2.45	49.83	0.89	2.42	11.0%
NC-01	2.52	61.82	2.76	50.15	0.91	2.17	−13.9%
NC-02	2.43	57.84	2.69	49.17	0.90	2.07	−14.8%
NC-03	2.31	52.53	2.60	50.08	0.89	2.49	7.8%

NC-00, NC-01, NC-02, and NC-03. In the present investigation, cracking first occurred in Mixture NC-00 at 114.3 h after casting. The absolute value of autogenous shrinkage at 114.3 h was 138, 70, 83, and 93 με for Mixture NC-00, NC-01, NC-02, and NC-03, which decreased by 49.3%, 39.9%, and 32.6% with increasing content of nano-$CaCO_3$ ranging from 0% to 1%, 2%, and 3%, respectively. Result shows that autogenous shrinkage decreased by adding nano-$CaCO_3$ to HSC. In addition, autogenous shrinkage of HSC containing 1% nano-$CaCO_3$ was the lowest, following by Mixture NC-02, NC-03, and NC-00. This is consistent with the previous investigation reporting that there is an optimal content of nano-$CaCO_3$ in reducing the autogenous shrinkage of cement-based materials [13]. The reduction of autogenous shrinkage by adding nano-$CaCO_3$ to HSC was due to the following reasons. Firstly, the addition of nano-$CaCO_3$ improves the microstructure of the concrete and increases the amount of calcium hydroxide in the cement paste. Calcium hydroxide is a byproduct of the hydration of cement, and it has been shown to help reduce the volume changes that occur during the curing process. By increasing the amount of calcium hydroxide in the cement paste, the volume changes can be reduced, leading to reduced autogenous shrinkage [69]. In addition, the nano-$CaCO_3$ mainly reacts with C_3A to form carboaluminates ($C_3A{\cdot}CaCO_3{\cdot}11H_2O$). The formed $C_3A{\cdot}CaCO_3{\cdot}11H_2O$ has the ability to expand slightly, which compensates the autogenous shrinkage of concrete [13]. One possible reason why the inhibitory effect of nano-$CaCO_3$ on autogenous shrinkage weakens with increasing content of nano-$CaCO_3$ would be that the specific surface area of nano-$CaCO_3$ is large, and increasing content makes it easy for the agglomeration of nano-$CaCO_3$ powders [9]. The air void content in concrete mixture would increase because of the nonuniform dispersion of nano-$CaCO_3$ powders, thus weakening the influence of nano-$CaCO_3$ on reducing autogenous shrinkage of concrete [70].

3.4. Influence of nano-$CaCO_3$ on restrained stress

The stress develops in concrete when the deformation is under restraint condition, and concrete will crack when restrained stress reaches its tensile capacity [40]. Fig. 11 depicts the results of restrained stress recorded in concrete specimens. Adding nano-$CaCO_3$ increased temperature rise rate and adiabatic temperature rise, which increased the thermal expansion, thus increasing the maximum compressive stress. The results of maximum compressive stress were −0.55, −1.17, −1.38, and −1.60 MPa, and the absolute value of which increased by 112.7%,

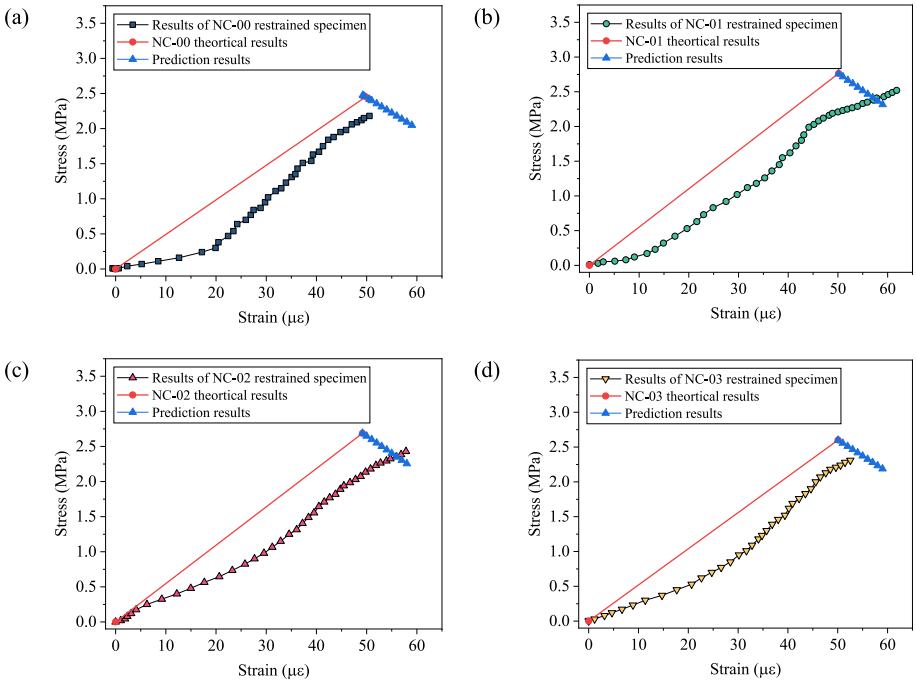

Fig. 19. Stress-strain relationships of four mixtures.

150.9%, and 190.9% with increasing content of nano-$CaCO_3$ ranging from 0% to 1%, 2%, and 3%, respectively. The restrained compressive stress and tensile stress developed quickly in the early stage of constant temperature phase and cooling phase, respectively. Then the restrained stress of concrete decreased slowly over time due to stress relaxation, as depicted in Fig. 11.

The compressive stress was transformed into the tensile one during cooling phase, and restrained tensile stress increased quickly because of the development of thermal deformation as well as shrinkage in HSC specimens. The sharp drop of stress curves in Fig. 11 represents that cracking occurred in the restrained specimens. Cracking stress is an index of tensile capacity of concrete under loading, which is defined as the stress when cracking occurs in the concrete during the test [71]. The cracking stress of Mixture NC-00, NC-01, NC-02, and NC-03 was 2.18, 2.52, 2.43, and 2.31 MPa at the cracking age of 114.3, 116.8, 115.9, and 114.6 h, respectively, which demonstrated that adding nano-$CaCO_3$ improved early-age cracking resistance of HSC. However, the cracking age and evolution of restrained tensile stress of different mixtures during the cooling phase were very similar. The possible reason would be that the addition of nano-$CaCO_3$ have an impact on the tensile creep potential of concrete. Specifically, the addition of nano-$CaCO_3$ decreased the tensile creep of concrete. This is because the addition of nano-$CaCO_3$ can increase the toughness of the material, causing it to undergo less deformation under tensile stress, thereby restricting the development of tensile creep. At the same time, the addition of nano-$CaCO_3$ increased the tensile strength and elastic modulus of concrete. Although the evolution of restrained tensile stress was slightly increased by adding nano-$CaCO_3$, the cracking ages of different mixtures were similar. Thus, the early-age cracking resistance of HSC could not be evaluated only by cracking stress or cracking age.

Hattel et al. and Liu et al. [72,73] estimate cracking resistance of concrete, and reflect damage degree of that using ratio of cracking stress to tensile strength. Considering that the curing condition of TSTM test was different from that of mechanical properties test. The actual age of concrete in TSTM test was converted to equivalent age at 20 °C with Eq. (9). The ratio of cracking stress to axial tensile strength at equivalent cracking age was taken to evaluate the early-age cracking resistance of HSC, as reported in Refs. [28,74].

$$t_e = \int_0^t \exp\left[\frac{E_a(T)}{R}\left(\frac{1}{T_{ref}+273}-\frac{1}{T(t)+273}\right)\right] dt \tag{9}$$

where t_e = equivalent age of 20 °C; $T(t)$ = actual temperature, in °C; $E_a(T)$ = activation energy, in kJ/mol; R = an ideal gas constant (8.315 J·mol^{-1}·K^{-1}); and T_{ref} = a reference temperature (20 °C). The equivalent cracking age was 299.70, 305.03, 350.17, and 401.24 h, and results of axial tensile strength at equivalent cracking age were 3.07, 3.46, 3.36, and 3.25 MPa for Mixture NC-00, NC-01, NC-02, and NC-03, respectively. The results of ratio of cracking stress to axial tensile strength at equivalent cracking age were 0.710, 0.728, 0.723, and 0.711, which increased by 2.5%, 1.8%, and 0.1% with increasing content of nano-$CaCO_3$ ranging from 0% to 1%, 2%, and 3%, respectively. The ratios of cracking stress to axial tensile strength at equivalent cracking age for four mixtures were in a range of 0.6–0.8, these results were in line with those of previous studies [75,76]. The main reason is that higher static fatigue and damage accumulation would be caused in restrained specimen due to the longer loading time of TSTM test than that of mechanical property test [77]. The great ratio of cracking stress to axial tensile strength at equivalent cracking age reflects a small damage degree and high cracking resistance of concrete specimens under loading. The results of cracking stress to axial tensile strength at equivalent cracking age indicated that Mixture NC-01 showed the highest cracking resistance than other mixtures.

3.5. Influence of nano-$CaCO_3$ on tensile creep

The restrained specimen was under full restraint condition, thus the deformation of restrained specimen was zero. Eq. (10) depicts the deformation of restrained specimen, which contains free shrinkage, creep, as well as elastic strain [17].

$$\varepsilon_{total} = \varepsilon_e + \varepsilon_{sh} + \varepsilon_{cr} = 0 \tag{10}$$

where ε_{total} = total deformation of restrained specimen, in με; ε_{sh} = free shrinkage of free specimen, in με; ε_e = accumulation of incremental elastic strain of restrained specimen, in με; and ε_{cr} = creep, in με. The results of total accumulated deformation recorded in restrained specimens and the results of creep are depicted in Figs. 12 and 13, respectively.

Fig. 13 depicts that compressive creep of concrete developed rapidly when the temperature rose due to hydration. Zhang et al. [39] report that around free expansion deformation is nearly compensated by creep in compression in the first 24 h, and similar results can be found in the present investigation, as depicted in Figs. 9 and 13. The compressive creep changed to the tensile one after that period because restrained tensile stress developed in restrained specimens when the concrete cooled down. In the present investigation, only tensile creep was discussed, and the tensile creep was zeroed at the time when restrained stress in tension occurred, as reported in Ref. [40]. Development of tensile creep of concrete specimens is depicted in Fig. 14. Mixture NC-00 cracked first at 114.3 h, and the tensile creep at that time was 150, 141, 144, and 146 με, which decreased by 6.0%, 4.0%, and 2.7%, respectively. When the tensile creep decreased, the long term part of the autogenous shrinkage would decrease accordingly due to the effect of capillary force. In general, the relationship between tensile creep and autogenous shrinkage is complex and depends on various factors, which needs to be investigated in further studies.

The creep-shrinkage ratio, which can be expressed as the ratio between the tensile creep to free shrinkage, was taken to estimate the creep behavior of HSC, as recommended in Ref. [53]. The creep-shrinkage ratio reveals the reduction in the development of tensile strain in concrete under restrained condition, which is used to evaluate the degree of stress relaxation. The shrinkage of free specimens at 114.3 h during the forced cooling phase was 200, 201, 200, 198 με, and the creep-shrinkage ratio at 114.3 h was 0.75, 0.70, 0.72, and 0.74, which decreased by 6.7%, 4.0%, and 1.3% with increasing content of nano-$CaCO_3$ ranging from 0% to 1%, 2%, and 3%, respectively, as depicted in Fig. 15. Adding nano-$CaCO_3$ led to a reduction in creep-shrinkage ratio, and the creep-shrinkage ratio of Mixture NC-01 was lower than that of the other mixtures.

The specific basic tensile creep is defined as the ratio of cumulative tensile creep to restrained stress considering that restrained stress developed with time in the present investigation [39,54]. Fig. 16 depicts the development of ratio of specific tensile creep to stress of HSC containing nano-$CaCO_3$. For Mixture NC-00, NC-01, NC-02, and NC-03, restrained stress at 114.3 h was 2.18, 2.43, 2.36, and 2.28 MPa, and specific tensile creep at 114.3 h was 68.62, 57.90, 61.02, and 64.17 με/MPa, which decreased by 15.6%, 11.1%, and 6.5% with increasing content of nano-$CaCO_3$ ranging from 0% to 1%, 2%, and 3%, respectively. Results indicated that visco-elastic properties of HSC under restraint condition were reduced by adding nano-$CaCO_3$, and Mixture NC-01 showed the lowest early-age visco-elastic response. Besides, specific tensile creep decreased nonlinearly with increasing content of nano-$CaCO_3$.

3.6. Influence of nano-$CaCO_3$ on cracking resistance

In the present investigation, two methods were taken to estimate cracking resistance of Mixture NC-00, NC-01, NC-02, and NC-03, respectively: 1) stress reserve, and 2) modified integrated criterion.

The stress reserve, which takes cracking stress as well as stress at room temperature of 20 °C into consideration simultaneously, is taken to evaluate cracking resistance of concrete by Shi et al. [26] and Zhang et al. [25], as depicted in Eq. (11) [78].

$$\varphi = \frac{\sigma_c - \sigma_r}{\sigma_c} \times 100\% \tag{11}$$

where φ = stress reserve; σ_c = cracking stress, in MPa; and σ_r = stress at room temperature (20 °C), in MPa.

Fig. 17 depicts that stress at room temperature was 1.98, 2.21, 2.14, and 2.07 MPa, and the result of stress reserve was 9.2%, 12.3%, 11.9%, and 10.4% for Mixture NC-00, NC-01, NC-02, and NC-03, which increased by 33.7%, 29.3%, and 13.0% with increasing content of nano-$CaCO_3$ ranging from 0% to 1%, 2%, and 3%, respectively.

In the present investigation, the integrated criterion was modified in Refs. [27,28] to compare influence of nano-$CaCO_3$ on cracking potential of HSC, as depicted in Eq. (12).

$$\varphi_N = \frac{S}{t_{tcr}} \tag{12}$$

where φ_N = integrated criterion of cracking potential, in MPa/(h·day), and all other variables were defined in Refs. [27,28]. Higher value of integrated criterion indicated higher cracking potential (lower cracking resistance).

Fig. 17 depicts that integrated criteria for Mixture NC-00, NC-01, NC-02, and NC-03 were 0.040, 0.028, 0.032, and 0.035 MPa/(h·day), which decreased by 30.0%, 20.0%, and 12.5% with increasing content of nano-$CaCO_3$ ranging from 0% to 1%, 2%, and 3%, respectively. The integrated criterion was the lowest when the content of nano-$CaCO_3$ was 1%. Results of stress reserve and integrated criterion indicated that adding nano-$CaCO_3$ increased early-age cracking resistance of HSC.

3.7. The simplified stress-strain failure criterion

The restrained specimen suffers sustained loading and creep, which resembles fatigue and creep failure [79]. When cracking occurs in concrete, cracking strain exceeds strain capacity. However, cracking stress is lower than strength capacity. To estimate safety of single restrained concrete considering the strain and stress of concrete, Zhu et al. [80] propose a stress-strain failure criterion based on results obtained from direct tensile test and restrained cracking test. In general, TSTM only has one motor to push and pull restrained specimen, thus, it is relatively inconvenient to carry out direct tension test on free specimen [20]. In the present investigation, the theoretical failure results obtained from prediction models were used to replace the results of direct tensile test in study [80], and the results of restrained cracking were obtained by TSTM. The usage of prediction models of mechanical properties to replace direct tensile test could simplify test procedure and reduce test cost, which made it more convenient for the application in practical engineering. The simplified stress-strain failure criterion is depicted in Eq. (13), and Fig. 18 depicts the stress-strain relationship between results of restrained cracking test and theoretical failure results.

$$f(\sigma_{cr}, \varepsilon_{cr}) = K \cdot E_p \cdot (\varepsilon_{cr} - \varepsilon_p) - (\sigma_p - \sigma_{cr}) \tag{13}$$

where $f(\sigma_{cr}, \varepsilon_{cr})$ = the simplified stress-strain failure criterion (concrete is safe when value of $f(\sigma_{cr}, \varepsilon_{cr})$ is less than 0, and concrete is likely to crack when value of $f(\sigma_{cr}, \varepsilon_{cr})$ is over 0); K = relationship between σ_{cr} and σ_p under the linear assumption, in MPa; σ_{cr} = stress of restrained concrete at the cracking age, in MPa; ε_{cr} = accumulative strain of restrained concrete at the cracking age, in με; σ_p = theoretical result of stress at equivalent cracking age, in MPa; and ε_p = theoretical result of strain at equivalent cracking age, in με.

The stress as well as strain of restrained concrete at the cracking age was determined on the TSTM. The theoretical results of stress σ_p as well as strain ε_p at equivalent cracking age were determined on the basis of the prediction models of axial tensile strength (Eq. (2)) as well as tensile elastic modulus (Eq. (3)), as depicted in Eq. (14).

$$\begin{cases} \sigma_p = \eta \cdot f_{t,28} \exp\left\{ -\lambda_1 [\ln(1 + (t_e - t_0))]^{-k_1} \right\} \\ \varepsilon_p = \dfrac{\sigma_p}{E_{t,28} \exp\left\{ -\lambda_2 [\ln(1 + (t_e - t_0))]^{-k_2} \right\}} \end{cases} \tag{14}$$

where η = relationship between cracking stress and tensile strength. Altoubat et al. [77] reveal that the cracking occurs when the stress in the concrete reaches around 80% of the tensile strength, and η was set as 0.8 in the present investigation.

The restrained cracking test was conducted to examine the prediction accuracy of the simplified stress-strain failure criterion proposed in the present investigation. The prediction result of σ_{pre} for four mixtures were determined by Eq. (13), as depicted in Table 5 and Fig. 19.

Table 5 depicts the theoretical failure results and results of restrained cracking test of Mixture NC-00, NC-01, NC-02, and NC-03, respectively. The predicted failure stress could be calculated by substituting the results of K, σ_p, ε_p, and ε_{cr} in Eq. (13). The relative prediction error ranged from −14.8% to 11.0%, which was acceptable in practical engineering, and was similar to the model with a prediction error ranged from −7.61% to 12.89% proposed by Zhu et al. [80]. Thus, the simplified stress-strain failure criterion could be used to predict the cracking stress of HSC containing nano-$CaCO_3$. Compared with the traditional strength and strain capacity criteria of concrete, simplified stress-strain failure criterion based on the results obtained from restrained cracking test and prediction models of mechanical properties was more applicable and convenient. In practical engineering, the simplified stress-strain failure criterion has certain significance to design a better temperature control strategy for increasing the cracking resistance of concrete.

4. Conclusions

The influence of nano-$CaCO_3$ on temperature history, autogenous shrinkage, restrained stress, and tensile creep of HSC was investigated, and the acting mechanism of nano-$CaCO_3$ on cracking failure behavior of HSC was explained from many aspects of material properties. The following conclusions could be obtained:

1. The compressive strength, splitting tensile strength, as well as elastic modulus of HSC were enhanced by adding nano-$CaCO_3$. The addition of 1% nano-$CaCO_3$ showed the optimum content, which gave the highest compressive, tensile strength and elastic modulus, followed by 2%, 3%, and 0%, respectively.
2. The autogenous shrinkage, tensile creep, creep-shrinkage ratio, as well as specific tensile creep of HSC were reduced by adding nano-$CaCO_3$. The autogenous shrinkage, tensile creep, creep-shrinkage ratio, as well as specific tensile creep of HSC containing 1% nano-$CaCO_3$ was the lowest, followed by HSC containing 2%, 3%, and 0%.
3. The early-age cracking resistance of HSC increased by adding nano-$CaCO_3$. Many criteria, e.g., cracking stress, ratio of cracking stress to axial tensile strength, stress reserve, as well as integrated criterion of cracking potential, were taken to evaluate early-age cracking resistance of HSC containing nano-$CaCO_3$.
4. The simplified stress-strain failure criterion was proposed. The relative prediction error ranged from −14.8% to 11.0%. Considering that the data was limited in the present investigation, future studies will be conducted using the criterion to better evaluate the cracking failure behavior of concrete in practical engineering.

Declaration of competing interest

The authors declare that they have no known competing financial interests or personal relationships that could have appeared to influence the work reported in this paper.

Data availability

Data will be made available on request.

Acknowledgements

The financial support of the National Natural Science Foundation of China (Grant No. 51879092) is gratefully acknowledged. The Post-graduate Research & Practice Innovation Program of Jiangsu Province (Grant No. KYCX22_0614) is also gratefully acknowledged. The support of the Fundamental Research Funds for the Central Universities (Grant No 2019B52814) is gratefully acknowledged.

References

[1] D.H. Wang, C.J. Shi, N. Farzadnia, Z.G. Shi, H.F. Jia, Z.H. Ou, A review on use of limestone powder in cement-based materials: mechanism, hydration and microstructures, Construct. Build. Mater. 181 (2018) 659–672, https://doi.org/10.1016/j.conbuildmat.2018.06.075.

[2] C. Liu, D.J. Shen, M. Li, C.C. Li, J.C. Kang, M.L. Wang, Investigation on the internal Relative humidity of superabsorbent polymer–modified concrete exposed to various ambient humidities at early age, J. Mater. Civ. Eng. 35 (4) (2023), https://doi.org/10.1061/(asce)mt.1943-5533.0004708.

[3] D. Cusson, T. Hoogeveen, An experimental approach for the analysis of early-age behaviour of high-performance concrete structures under restrained shrinkage, Cement Concr. Res. 37 (2) (2007) 200–209, https://doi.org/10.1016/j.cemconres.2006.11.005.

[4] D.J. Shen, J.C. Kang, C. Liu, M. Li, Y.F. Wei, L.K. Zhou, Effect of temperature rise inhibitor on early-age behavior and cracking resistance of high strength concrete under uniaxial restrained condition, J. Build. Eng. 64 (2023), 105588, https://doi.org/10.1016/j.jobe.2022.105588.

[5] N. Banthia, N. Nandakumar, Crack growth resistance of hybrid fiber reinforced cement composites, Cem. Concr. Compos. 25 (1) (2003) 3–9, https://doi.org/10.1016/S0958-9465(01)00043-9.

[6] B.W. Jo, C.H. Kim, G.H. Tae, J.B. Park, Characteristics of cement mortar with nano-SiO_2 particles, Construct. Build. Mater. 21 (6) (2007) 1351–1355, https://doi.org/10.1016/j.conbuildmat.2005.12.020.

[7] M. Cao, X. Ming, K. He, L. Li, S. Shen, Effect of macro-, micro- and nano-calcium carbonate on properties of cementitious composites-A review, Materials 12 (5) (2019), https://doi.org/10.3390/ma12050781.

[8] A.A. Ramezanianpour, E. Ghiasvand, I. Nickseresht, M. Mahdikhani, F. Moodi, Influence of various amounts of limestone powder on performance of Portland limestone cement concretes, Cem. Concr. Compos. 31 (10) (2009) 715–720, https://doi.org/10.1016/j.cemconcomp.2009.08.003.

[9] I. Ahmad, D. Shen, K.A. Khan, A. Jan, M. Khubaib, T. Ahmad, H. Nasir, Effectiveness of limestone powder in controlling the shrinkage behavior of cement based system: a review, Silicon (2021), https://doi.org/10.1007/s12633-020-00897-1.

[10] X.Y. Liu, L. Chen, A.H. Liu, X.R. Wang, Effect of nano-$CaCO_3$ on properties of cement paste, Energy Proc. 16 (2012) 991–996, https://doi.org/10.1016/j.egypro.2012.01.158.

[11] T. Meng, Y. Yu, Z. Wang, Effect of nano-$CaCO_3$ slurry on the mechanical properties and micro-structure of concrete with and without fly ash, Compos. B Eng. 117 (2017) 124–129, https://doi.org/10.1016/j.compositesb.2017.02.030.

[12] T. Sato, F. Diallo, Seeding effect of nano-$CaCO_3$ on the hydration of tricalcium silicate, Transport. Res. Rec.: J. Transport. Res. Board 2141 (1) (2010) 61–67, https://doi.org/10.3141/2141-11.

[13] X.Y. Liu, T.C. Fang, J.Q. Zuo, Effect of nano-materials on autogenous shrinkage properties of cement based materials, Symmetry 11 (9) (2019), https://doi.org/10.3390/sym11091144.

[14] D.J. Shen, C. Liu, J.C. Kang, Q. Yang, M. Li, C.C. Li, X. Zeng, Early-age autogenous shrinkage and tensile creep of hooked-end steel fiber reinforced concrete with different thermal treatment temperatures, Cem. Concr. Compos. 131 (2022) 104550,, https://doi.org/10.1016/j.cemconcomp.2022.104550.

[15] I. Pane, W. Hansen, Predictions and verifications of early-age stress development in hydrating blended cement concrete, Cement Concr. Res. 38 (11) (2008) 1315–1324, https://doi.org/10.1016/j.cemconres.2008.05.001.

[16] J.C. Kang, D.J. Shen, C. Liu, M. Li, C.Y. Wen, X. Shi, Early-age autogenous shrinkage and cracking risk of 5D hooked-end steel fibre reinforced high strength concrete under uniaxial restrained condition, J. Mater. Civ. Eng. (2023), https://doi.org/10.1061/JMCEE7/MTENG-15446.

[17] K. Kolver, S. Igarashi, A. Bentur, Tensile creep behavior of high strength concretes at early ages, Mater. Struct. 32 (5) (1999) 383–387, https://doi.org/10.1007/BF02479631.

[18] S. Igarashi, A. Bentur, K. Kovler, Autogenous shrinkage and induced restraining stresses in high-strength concretes, Cement Concr. Res. 30 (11) (2000) 1701–1707, https://doi.org/10.1016/S0008-8846(00)00399-9.

[19] T.J. Barrett, I. De la Varga, W.J. Weiss, Reducing cracking in concrete structures by using internal curing with high volumes of fly ash, Structures Congress 2012 (2012) 699–707, https://doi.org/10.1061/9780784412367.063.

[20] K. Kovler, Testing system for determining the mechanical behaviour of early age concrete under restrained and free uniaxial shrinkage, Mater. Struct. 27 (6) (1994) 324–330, https://doi.org/10.1007/BF02473424.

[21] A.E. Klausen, T. Kanstad, Ø. Bjøntegaard, Updated temperature-stress testing machine (TSTM): introductory tests, calculations, verification, and investigation of variable fly ash content, CONCREEP 10 (2015) 724–732.

[22] K.A. Riding, J.L. Poole, A.K. Schindler, M.C. Juenger, K.J. Folliard, Quantification of effects of fly ash type on concrete early-age cracking, ACI Mater. J. 105 (2) (2008) 149–155.

[23] S. Tongaroonsri, S. Tangtermsirikul, Effect of mineral admixtures and curing periods on shrinkage and cracking age under restrained condition, Construct. Build. Mater. 23 (2) (2009) 1050–1056, https://doi.org/10.1016/j.conbuildmat.2008.05.023.

[24] T. Meagher, N. Shanahan, D. Buidens, K.A. Riding, A. Zayed, Effects of chloride and chloride-free accelerators combined with typical admixtures on the early-age cracking risk of concrete repair slabs, Construct. Build. Mater. 94 (2015) 270–279, https://doi.org/10.1016/j.conbuildmat.2015.07.003.

[25] G.Z. Zhang, L.Q. Tu, W.H. Xia, K.X. Liu, B.J. Liu, Study on evaluation index of early ages cracking in concrete, Concrete 5 (37) (2005) 13–17 (in Chinese).

[26] N.N. Shi, J.S. Ouyang, R.X. Zhang, D.H. Huang, Experimental study on early-age crack of mass concrete under the controlled temperature history, Adv. Mater. Sci. Eng. 12 (3) (2014) 352–358, https://doi.org/10.1155/2014/671795.

[27] D.J. Shen, J.L. Jiang, J.X. Shen, P.P. Yao, G.Q. Jiang, Influence of prewetted lightweight aggregates on the behavior and cracking potential of internally cured concrete at an early age, Construct. Build. Mater. 99 (2015) 260–271, https://doi.org/10.1016/j.conbuildmat.2015.08.093.

[28] D.J. Shen, J.C. Kang, Y. Jiao, M. Li, C.C. Li, Effects of different silica fume dosages on early-age behavior and cracking resistance of high strength concrete under restrained condition, Construct. Build. Mater. 263 (2020), 120218, https://doi.org/10.1016/j.conbuildmat.2020.120218.

[29] Chinese Standard GB 175-2007/XG1-2018, Common Portland Cement, Standard press of China, Beijing, China, 2018 (in Chinese).

[30] ASTM C150/C150M-20, Standard Specification for Portland Cement, ASTM International, West Conshohocken, PA, 2020.

[31] Chinese Standard GB/T 50081-2019, Standard for Test Methods of Concrete Physical and Mechanical Properties, Standard press of China, Beijing, China, 2019 (in Chinese).

[32] A. Darquennes, S. Staquet, M.-P. Delplancke-Ogletree, B. Espion, Effect of autogenous deformation on the cracking risk of slag cement concretes, Cem. Concr. Compos. 33 (3) (2011) 368–379, https://doi.org/10.1016/j.cemconcomp.2010.12.003.

[33] D.H. Nguyen, V.T. Nguyen, P. Lura, V.T. Dao, Temperature-stress testing machine-A state-of-the-art design and its unique applications in concrete research, Cem. Concr. Compos. 102 (2019) 28–38, https://doi.org/10.1016/j.cemconcomp.2019.04.019.

[34] D.J. Shen, C. Liu, C.Y. Wen, J.C. Kang, M. Li, H. Jiang, Restrained cracking failure behavior of concrete containing MgO compound expansive agent under adiabatic condition at early age, Cem. Concr. Compos. 135 (2022) 104825, https://doi.org/10.1016/j.cemconcomp.2022.104825.

[35] K. Tang, S. Millard, G. Beattie, Technical and economic aspects of using GGBFS for crack control mitigation in long span reinforced concrete structures, Construct. Build. Mater. 39 (2013) 65–70, https://doi.org/10.1016/j.conbuildmat.2012.05.012.

[36] D. Cusson, W.L. Repette, Early-age cracking in reconstructed concrete bridge barrier walls, ACI Mater. J. 97 (4) (2000) 438–446.

[37] ACI Committee 207, Effect of Restraint, Volume Change and Reinforcement on Cracking of Mass Concrete, 1995.

[38] V.T. Giner, S. Ivorra, F.J. Baeza, E. Zornoza, B. Ferrer, Silica fume admixture effect on the dynamic properties of concrete, Construct. Build. Mater. 25 (8) (2011) 3272–3277, https://doi.org/10.1016/j.conbuildmat.2011.03.014.

[39] D.J. Shen, C. Liu, Y.Y. Luo, H.Z. Shao, X.Y. Zhou, S.L. Bai, Early-age autogenous shrinkage, tensile creep, and restrained cracking behavior of ultra-high-performance concrete incorporating polypropylene fibers, Cem. Concr. Compos. 138 (2023). https://doi.org/10.1016/j.cemconcomp.2023.104948.

[40] D.J. Shen, W.T. Wang, Q.Y. Li, P.P. Yao, G.Q. Jiang, Early-age behaviour and cracking potential of fly ash concrete under restrained condition, Mag. Concr. Res. 72 (5) (2020) 246–261, https://doi.org/10.1680/jmacr.18.00106.

[41] D. Cusson, T. Hoogeveen, Internal curing of high-performance concrete with pre-soaked fine lightweight aggregate for prevention of autogenous shrinkage cracking, Cement Concr. Res. 38 (6) (2008) 757–765, https://doi.org/10.1016/j.cemconres.2008.02.001.

[42] F.U.A. Shaikh, S.W.M. Supit, Mechanical and durability properties of high volume fly ash (HVFA) concrete containing calcium carbonate ($CaCO_3$) nanoparticles, Construct. Build. Mater. 70 (2014) 309–321, https://doi.org/10.1016/j.conbuildmat.2014.07.099.

[43] S. Mishra, S.H. Sonawane, R.P. Singh, Studies on characterization of nano $CaCO_3$ prepared by the in situ deposition technique and its application in PP-nano $CaCO_3$ composites, J. Polym. Sci., Part B: Polym. Phys. 43 (1) (2005) 107–113, https://doi.org/10.1002/polb.20296.

[44] T. Kanstad, T.A. Hammer, Ø. Bjøntegaard, E.J. Sellevold, Mechanical properties of young concrete: Part I: experimental results related to test methods and temperature effects, Mater. Struct. 36 (4) (2003) 218–225, https://doi.org/10.1007/BF02479614.

[45] T. Kanstad, T.A. Hammer, Ø. Bjøntegaard, E.J. Sellevold, Mechanical properties of young concrete: Part II: determination of model parameters and test program

proposals, Mater. Struct. 36 (4) (2003) 226–230, https://doi.org/10.1007/BF02479615.
[46] T. Sato, J. Beaudoin, Effect of nano-$CaCO_3$ on hydration of cement containing supplementary cementitious materials, Adv. Cement Res. 23 (1) (2011) 33–43, https://doi.org/10.1680/adcr.9.00016.
[47] P. Lura, Autogenous Deformation and Internal Curing of Concrete, Dup Science, 2003.
[48] H.T. See, E.K. Attiogbe, M.A. Miltenberger, Shrinkage cracking characteristics of concrete using ring specimens, Materials J. 100 (3) (2003) 239–245.
[49] T. Wee, H. Lu, S. Swaddiwudhipong, Tensile strain capacity of concrete under various states of stress, Mag. Concr. Res. 52 (3) (2000) 185–193, https://doi.org/10.1680/macr.2000.52.3.185.
[50] H. Assaedi, T. Alomayri, C.R. Kaze, B.B. Jindal, S. Subaer, F. Shaikh, S. Alraddadi, Characterization and properties of geopolymer nanocomposites with different contents of nano-CaCO3, Construct. Build. Mater. 252 (2020), 119137, https://doi.org/10.1016/j.conbuildmat.2020.119137.
[51] P. Lura, J. Bisschop, On the origin of eigenstresses in lightweight aggregate concrete, Cem. Concr. Compos. 26 (5) (2004) 445–452, https://doi.org/10.1016/S0958-9465(03)00072-6.
[52] D.J. Shen, X.Z. Liu, Q.Y. Li, L. Sun, W.T. Wang, Early-age behavior and cracking resistance of high-strength concrete reinforced with Dramix 3D steel fiber, Construct. Build. Mater. 196 (2019) 307–316, https://doi.org/10.1016/j.conbuildmat.2018.10.125.
[53] D.J. Shen, C. Liu, C.C. Li, X.G. Zhao, G.Q. Jiang, Influence of Barchip fiber length on early-age behavior and cracking resistance of concrete internally cured with super absorbent polymers, Construct. Build. Mater. 214 (2019) 219–231, https://doi.org/10.1016/j.conbuildmat.2019.03.209.
[54] D.J. Shen, J.L. Jiang, M.Y. Zhang, P.P. Yao, G.Q. Jiang, Tensile creep and cracking potential of high performance concrete internally cured with super absorbent polymers at early age, Construct. Build. Mater. 165 (2018) 451–461, https://doi.org/10.1016/j.conbuildmat.2017.12.136.
[55] J. Camiletti, A.M. Soliman, M.L. Nehdi, Effect of nano-calcium carbonate on early-age properties of ultra-high-performance concrete, Mag. Concr. Res. 65 (5) (2013) 297–307, https://doi.org/10.1680/macr.12.00015.
[56] K. De Weerdt, M.B. Haha, G. Le Saout, K.O. Kjellsen, H. Justnes, B. Lothenbach, Hydration mechanisms of ternary Portland cements containing limestone powder and fly ash, Cement Concr. Res. 41 (3) (2011) 279–291, https://doi.org/10.1016/j.cemconres.2010.11.014.
[57] D.J. Shen, C. Liu, Z.Z. Feng, S.S. Zhu, C. Liang, Influence of ground granulated blast furnace slag on the early-age anti-cracking property of internally cured concrete, Construct. Build. Mater. 223 (2019) 233–243, https://doi.org/10.1016/j.conbuildmat.2019.06.149.
[58] J. Schlitter, A. Senter, D. Bentz, T. Nantung, W. Weiss, A dual concentric ring test for evaluating residual stress development due to restrained volume change, J. ASTM Int. (JAI) 7 (9) (2010) 1–13, https://doi.org/10.1520/JAI103118.
[59] K. Raoufi, J. Schlitter, D.P. Bentz, W.J. Weiss, Parametric assessment of stress development and cracking in internally cured restrained mortars experiencing autogenous deformations and thermal loading, Adv. Civ. Eng. (2011) 1–16, https://doi.org/10.1155/2011/870128.
[60] A. Darquennes, S. Staquet, B. Espion, Determination of time-zero and its effect on autogenous deformation evolution, Eur. J. Environ. Civ. En. 15 (7) (2011) 1017–1029, https://doi.org/10.1080/19648189.2011.9695290.
[61] H. Huang, G. Ye, Examining the "time-zero" of autogenous shrinkage in high/ultra-high performance cement pastes, Cement Concr. Res. 97 (2017) 107–114, https://doi.org/10.1016/j.cemconres.2017.03.010.
[62] Y. Ma, X. Yang, J. Hu, Z. Zhang, H. Wang, Accurate determination of the "time-zero" of autogenous shrinkage in alkali-activated fly ash/slag system, Compos. B Eng. 177 (2019), 107367, https://doi.org/10.1016/j.compositesb.2019.107367.
[63] J.R. Tenório Filho, M.A. Pereira Gomes de Araújo, D. Snoeck, N. De Belie, Discussing different approaches for the time-zero as start for autogenous shrinkage in cement pastes containing superabsorbent polymers, Materials 12 (18) (2019) 2962–2977, https://doi.org/10.3390/ma12182962.
[64] M.S. Meddah, A. Tagnit-Hamou, Evaluation of rate of deformation for early-age concrete shrinkage analysis and time zero determination, J. Mater. Civ. Eng. 23 (7) (2011) 1076–1086, https://doi.org/10.1061/(ASCE)MT.1943-5533.0000261.
[65] P. Lura, K. Van Breugel, I. Maruyama, Effect of curing temperature and type of cement on early-age shrinkage of high-performance concrete, Cement Concr. Res. 31 (12) (2001) 1867–1872, https://doi.org/10.1016/S0008-8846(01)00601-9.
[66] C.H. Jiang, Y. Yang, Y. Wang, Y.N. Zhou, C.C. Ma, Autogenous shrinkage of high performance concrete containing mineral admixtures under different curing temperatures, Construct. Build. Mater. 61 (2014) 260–269, https://doi.org/10.1016/j.conbuildmat.2014.03.023.
[67] L.M. Wu, N. Farzadnia, C.J. Shi, Z.H. Zhang, H. Wang, Autogenous shrinkage of high performance concrete: a review, Construct. Build. Mater. 149 (2017) 62–75, https://doi.org/10.1016/j.conbuildmat.2017.05.064.
[68] I. Chu, S.H. Kwon, M.N. Amin, J.-K. Kim, Estimation of temperature effects on autogenous shrinkage of concrete by a new prediction model, Construct. Build. Mater. 35 (2012) 171–182, https://doi.org/10.1016/j.conbuildmat.2012.03.005.
[69] X. Qian, J.L. Wang, L. Wang, Y. Fang, Enhancing the performance of metakaolin blended cement mortar through in-situ production of nano to sub-micro calcium carbonate particles, Construct. Build. Mater. 196 (2019) 681–691, https://doi.org/10.1016/j.conbuildmat.2018.11.134.
[70] F.M. Nejad, M. Tolouei, H. Nazari, A. Naderan, Effects of calcium carbonate nanoparticles and fly ash on mechanical and permeability properties of concrete, Advances in Civil Engineering Materials 7 (1) (2018) 651–668, https://doi.org/10.1520/ACEM20180066.
[71] J.D. Xin, G.X. Zhang, Y. Liu, Z.H. Wang, Z. Wu, Evaluation of behavior and cracking potential of early-age cementitious systems using uniaxial restraint tests: a review, Construct. Build. Mater. 231 (2020), 117146, https://doi.org/10.1016/j.conbuildmat.2019.117146.
[72] J.H. Hattel, J. Thorborg, A numerical model for predicting the thermomechanical conditions during hydration of early-age concrete, Appl. Math. Model. 27 (1) (2003) 1–26, https://doi.org/10.1016/S0307-904X(02)00082-3.
[73] L. Liu, J. Ouyang, F. Li, J. Xin, D. Huang, S. Gao, Research on the crack risk of early-age concrete under the temperature stress test machine, Materials 11 (10) (2018). doi:10.3390/ma11101822.
[74] M. Krauß, F.S. Rostásy, A.W. Gutsch, Modelling of Degree of Hydration on Basis of Adiabatic Heat Release, 2001. IPACS REPORT BE96-3843.
[75] K.A. Riding, J.L. Poole, A.K. Schindler, M.C. Juenger, K.J. Folliard, Effects of construction time and coarse aggregate on bridge deck cracking, ACI Mater. J. 106 (5) (2009) 448–454.
[76] Ø. Bjøntegaard, E. Sellevold, Capabilities and limitations, in: International RILEM Symposium on Concrete Science and Engineering: A Tribute to Arnon Bentur, RILEM Publications SARL, 2004.
[77] S.A. Altoubat, D.A. Lange, Creep, shrinkage, and cracking of restrained concrete at early age, ACI Mater. J. 98 (4) (2001) 323–331.
[78] D.J. Shen, J.L. Jiang, J.X. Shen, P.P. Yao, G.Q. Jiang, Influence of curing temperature on autogenous shrinkage and cracking resistance of high-performance concrete at an early age, Construct. Build. Mater. 103 (2016) 67–76, https://doi.org/10.1016/j.conbuildmat.2015.11.039.
[79] J. Hümme, C. von der Haar, L. Lohaus, S. Marx, Fatigue behaviour of a normal-strength concrete – number of cycles to failure and strain development, Struct. Concr. 17 (4) (2016) 637–645, https://doi.org/10.1002/suco.201500139.
[80] H. Zhu, Y. Hu, Q.B. Li, R. Ma, Restrained cracking failure behavior of concrete due to temperature and shrinkage, Construct. Build. Mater. 244 (2020), https://doi.org/10.1016/j.conbuildmat.2020.118318.